Strain and size effects on heat transport in nanostructures

Cite as: Journal of Applied Physics **93**, 3535 (2003); https://doi.org/10.1063/1.1555256
Submitted: 12 November 2002 . Accepted: 27 December 2002 . Published Online: 05 March 2003

R. C. Picu, T. Borca-Tasciuc, and M. C. Pavel

Strain and size effects on heat transport in nanostructures

R. C. Picu,[a] T. Borca-Tasciuc, and M. C. Pavel
Department of Mechanical, Aerospace and Nuclear Engineering, Rensselaer Polytechnic Institute, Troy, New York 12180

(Received 12 November 2002; accepted 27 December 2002)

The relative role of the residual strain and dimensional scaling on heat transport in nanostructures is investigated by molecular dynamics simulations of a model Lennard-Jones solid. It is observed that tensile (compressive) strains lead to a reduction (enhancement) of the lattice thermal conductivity. A nonhydrostatic strain induces thermal conductivity anisotropy in the material. This effect is due to the variation with strain of the stiffness tensor and lattice anharmonicity, and therefore of the phonon group velocity and phonon mean free path. The effect due to the lattice anharmonicity variation appears to be dominant. The size effect was studied separately in unstrained thin films. Phonon scattering on surfaces leads to a drastic reduction of the thermal conductivity effect which is much more important than that due to strain in the bulk. It is suggested that strain may be used to tailor the phonon mean free path which offers an indirect method to control the size effect. © *2003 American Institute of Physics.* [DOI: 10.1063/1.1555256]

I. INTRODUCTION

It has been long recognized that hydrostatic pressure influences heat transport in solids. Relatively well understood[1–4] is the thermal conductivity reduction at low temperatures due to phonon scattering by the stress-split states of donors/acceptors in doped semiconductors under uniaxial deformation. However, at and above room temperature, the lattice thermal conductivity may increase with applied hydrostatic pressure as reported in a number of experimental studies performed in semiconductors and ionic lattice materials.[5–9] Although the fundamentals of the physics of heat transport in bulk materials are relatively well understood,[10–13] the effects of strain fields on the intrinsic lattice thermal conductivity have been only qualitatively studied.[14] No quantitative models exist to assert the effects of strain on lattice thermal conductivity at elevated temperatures. The observed increase in lattice thermal conductivity under pressure was qualitatively explained within the formalism of anharmonic three-phonon interaction model,[15] by assuming a possible increase in the characteristic Debye temperature and/or a reduction in the Gruneissen parameter.

Nanostructures, such as quantum wells and superlattices, may carry residual strains much larger than those typically found in the similar bulk material. For instance, a $\sim 2\%$ strain is sustained within the layers of symmetrized strain Si/Ge superlattices, while bulk single crystal silicon may only carry a residual strain an order of magnitude smaller. It is therefore interesting to investigate to what extent strain may be used to tailor the thermal transport properties for specific applications. For instance, while high thermal conductivity is beneficial for the thermal management of lasers and microelectronics which generate a considerable amount of heat that must be dissipated, low thermal conductivity is required by thermoelectric applications in order to increase the energy conversion efficiency. On the other hand, as structures approach dimensions comparable to the characteristic length scales of heat carriers, effects due to phonon interference and scattering on boundaries and interfaces start playing an important role.[16–21] Therefore, in order to improve control over heat transport in nanostructures, the relative importance of the strain and size effects must be clarified.

A study of this topic is presented in this article. The thermal conductivity of a model Lennard-Jones (LJ) solid is evaluated in molecular dynamics simulations. The solid is subjected to hydrostatic, as well as to deviatoric strain, corresponding to plane strain and plane stress conditions, in separate simulations. In order to avoid surface scattering, periodic boundary conditions are used in these models. Then, a thin film is considered, in which the strain state approaches that of plane stress, and in which phonon scattering on surfaces is allowed. The computed thermal conductivity variation with respect to the bulk is analyzed. The article is organized as follows: the modeling and simulation procedure is presented in Sec. II, while the results are presented and discussed in Sec. III. The conclusions are summarized in closure.

II. MODELING AND SIMULATION FRAMEWORK

The material considered here is a monatomic Lennard-Jones solid. The interatomic interactions are described by the potential

$$u(r)=\begin{cases} 4\varepsilon_{\mathrm{LJ}}\left(\left(\dfrac{\sigma_{\mathrm{LJ}}}{r}\right)^{12}-\left(\dfrac{\sigma_{\mathrm{LJ}}}{r}\right)^{6}\right) & r\leqslant R_c \\ u(R_c) & r>R_c \end{cases}, \tag{1}$$

where r denotes the distance between any pair of atoms. The cutoff radius is chosen to be $R_c=2.1\sigma_{\mathrm{LJ}}$, the potential including both a repulsive and an attractive branch. The units of length, energy and time of the problem are, respectively,

[a]Author to whom correspondence should be addressed; electronic mail: picuc@rpi.edu

σ_{LJ}, ε_{LJ} and $\sigma_{LJ}\sqrt{m_0/\varepsilon_{LJ}}$, where m_0 is the atomic mass. The units employed for stress are $\varepsilon_{LJ}/\sigma_{LJ}^3$, while those for thermal conductivity are $k_B/\sigma^2\sqrt{\varepsilon/m_0}$.

With proper calibration, the model corresponds to various materials that allow representation by a pair potential. For example, with $\varepsilon_{LJ}=119.8k_B$ and $\sigma_{LJ}=3.405$ Å, the material corresponds to solid Ar.

The atoms are arranged in a fcc lattice with lattice parameter chosen such to render the pressure zero at the imposed temperature. Periodic boundary conditions are used in all simulations, except for the case of the free standing thin film. The system is evolved in equilibrium by integrating the equations of motion of all particles. The integration algorithm and the thermostat are those due to Berendsen, Postma, and van Gunsteren.[22]

The lattice thermal conductivity (k) is computed in equilibrium constant energy simulations based on the fluctuation dissipation theorem of linear response theory, using the Green–Kubo equation[23]

$$\kappa=\frac{V}{3k_BT^2}\int_0^\infty \langle \mathbf{q}(t)\cdot\mathbf{q}(0)\rangle dt. \tag{2}$$

Here, V is the volume of the simulation cell, T is the temperature, and the angular parentheses stand for the heat flux ($\mathbf{q}$) autocorrelation function. The heat flux is computed from

$$\mathbf{q}(t)=\frac{1}{2V}\sum_{i=1}^{N}\sum_{j=1}^{N}\mathbf{r}_{ij}\cdot(\mathbf{F}_{ij}\cdot\mathbf{v}_{ij}), \tag{3}$$

where $\mathbf{r}_{ij}$ and $\mathbf{F}_{ij}$ are the vector distance and the force acting between atoms i and j, and $\mathbf{v}_i$ is the velocity of atom i. The convective contribution to the heat flux was neglected as appropriate in a solid.

The thermal conductivity is a tensor relating the heat flux and the temperature gradient in Fourier's law, $q_\alpha=-\Sigma_\beta\kappa_{\alpha\beta}\partial T/\partial x_\beta$. In this fcc lattice and in the absence of any strain field, the thermal conductivity tensor should follow the cubic symmetry of the lattice. The thermal conductivity in Eq. (2) is the scalar value obtained by averaging the conductivity in the three principal directions. The averaging was performed in cases that exhibit the appropriate symmetry, i.e., the unloaded bulk and the material subjected to hydrostatic strain. In all other cases, the directional thermal conductivity was computed by integrating the autocorrelation function of the respective component of the heat flux.

The integration of Eq. (2) raises some problems due to the long tails of the autocorrelation function. The statistical noise was reduced by averaging over replicas of the system. The autocorrelation function shows an initial fast decay due to the optical modes of the crystal. These modes do not contribute significantly to heat transport and to the lattice thermal conductivity. The subsequent decay is slow and is due to long wavelength phonon scattering.

The thermal conductivity is obtained by direct integration of the autocorrelation function. The autocorrelation function needs to be computed over a long time, approximately 500 000 steps in these simulations, which corresponds to 1 ns of real time if the Ar conversion of the LJ units is used. The correlation function decays to zero before the 1 ns limit. This procedure led to error bars on the order of 15%–20% on the computed thermal conductivity. The results presented in the next section are normalized by the thermal conductivity of the material in its stress-free state. This value was obtained with much better accuracy (estimated to be 5%) by considering many replicas of the system, in order to prevent error amplification during normalization.

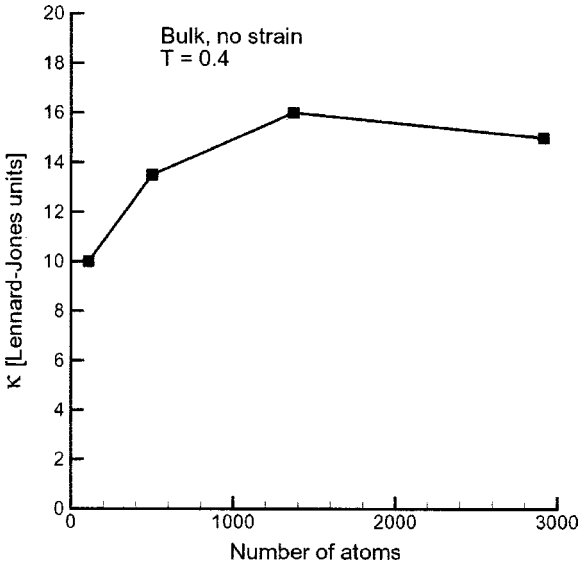

FIG. 1. Simulation cell size effect on the computed lattice thermal conductivity of an unloaded bulk Lennard-Jones solid (fcc) at $T=0.4$ (LJ temperature units). The thermal conductivity reaches a constant value once the model contains more than 1000 atoms. The error bar for the largest model considered ($N=3000$ atoms) is ±1 Lennard-Jones units of thermal conductivity.

An alternative to this approach is the fitting of two exponentials to the computed autocorrelation function, one corresponding to the fast initial decay, and the other capturing the tail of the function. This procedure was attempted, but the fit is not satisfactory. In fact, other authors similarly observed that the long time decay is not accurately represented by an exponential.[24,25]

The selection of the simulation cell size requires some care, since the use of periodic boundary conditions effectively truncates the phonon spectrum to wavelengths shorter than the model size. If the simulation cell is too small, the tail of the correlation function is affected by image effects. The upper limit of the model size is imposed by computational power limitations. To determine the appropriate size, the thermal conductivity of the bulk unstrained material (zero pressure) at $T=0.4$ (Lennard-Jones units) was evaluated in models of increasing size. The results are shown in Fig. 1. When the cell contains more than $N=1000$ atoms, the results become independent of the model size at this temperature. The error bar on the largest model is ±1 LJ unit in these runs. A model containing $N=864$ atoms ($6\times6\times6$ fcc unit cells) was selected for further simulations.

The predictions of the model were compared with other published results and with experimental data. Figure 2 shows the variation of the computed thermal conductivity with temperature along with similar data reported by Kaburaki, Li,

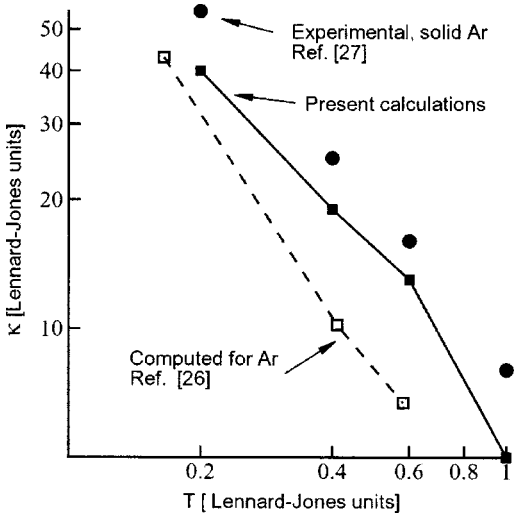

FIG. 2. Variation of the lattice thermal conductivity with temperature. Numerical data (see Ref. 26) are included along with experimental values for Ar (see Ref. 27). The experimental data have been rendered nondimensional (Lennard-Jones units) for easy comparison with the numerical results.

and Yip.[26] Experimental data for solid Ar[27] are included. The experimental data are nondimensionalized for easy comparison with the corresponding Lennard-Jones quantity. The present results are in reasonable agreement with the experimental data. Furthermore, it is seen that, for this range of temperature, the thermal conductivity decreases with temperature, which indicates that phonon–phonon scattering processes dominate.

III. RESULTS AND DISCUSSION

Figure 3 shows the normalized lattice thermal conductivity under hydrostatic strain. The normalization is made with the lattice thermal conductivity of the un-deformed bulk

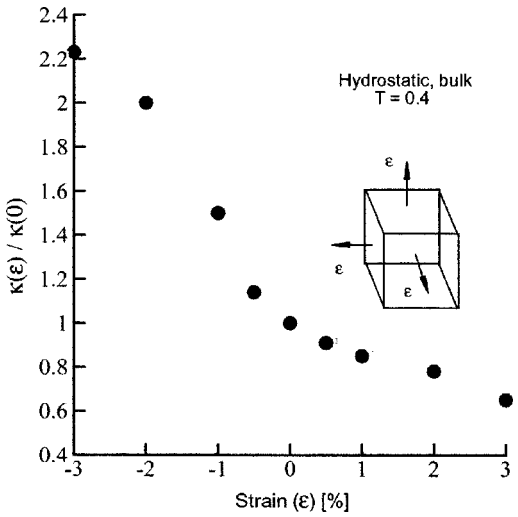

FIG. 3. Variation of the normalized thermal conductivity with hydrostatic strain. The normalization is made with the bulk thermal conductivity corresponding to zero strain. The strain values on the horizontal axis represent strain in one spatial direction. The principal directions of strain are aligned with the ⟨100⟩ crystallographic axes. The inset shows the type of loading. The error bars on all quantities are 20%.

at the same temperature. The conductivity increases under compression and decreases under dilatation, with compression inducing a larger effect. The effect can be qualitatively understood from the kinetic theory.

In the kinetic theory, the thermal conductivity is proportional to the specific heat capacity, the phonon group velocity and the phonon mean free path. Since the experiment is performed above Debye temperature, the specific heat capacity is assumed to be constant. On the other hand, the phonon group velocity is taken to be the speed of sound in the respective material because only long wavelength phonons contribute significantly to thermal energy transport. The speed of sound is proportional to the square root of the stiffness which, due to the nonlinear character of lattice elasticity, changes significantly with strain. Moreover, the phonon mean free path is controlled by the lattice anharmonicity which is also affected by strain.

These parameters respond differently to strain. The stiffness increases in compression and decreases in tension, as dictated by the functional form of the interatomic potential. In this material and crystal orientation, −3% hydrostatic strain (compression) leads to 61% increase of the stiffness, while +3% strain corresponds to a 32% reduction of this parameter. Through the variation of the group velocity with strain, this corresponds, respectively, to 27% increase and 18% decrease in thermal conductivity. More than 100% increase in thermal conductivity is calculated for −3% compression, and a 40% reduction is estimated for 3% dilation. Hence, the anharmonicity-induced mean free path variation with strain appears to play a major role in defining the strain dependence of the thermal conductivity.

The effect of a nonhydrostatic strain state was further investigated in the bulk. Plane strain conditions defined by an imposed biaxial in-plane strain and zero out-of-plane strain were considered. The principal axes of strain were taken to be aligned with the principal crystallographic axes, the ⟨100⟩ directions. The thermal conductivity was evaluated in each principal direction. The results are shown in Fig. 4, in which the in-plane normalized thermal conductivity is obtained by averaging over the two in-plane principal directions. The data in Fig. 3 corresponding to the hydrostatic case are shown for reference. The strain on the horizontal axis represents strain imposed in a given principal in-plane direction, while the normalization of the vertical axis is made with the thermal conductivity of the bulk at zero pressure and same temperature ($T=0.4$). Strain affects the in-plane thermal conductivity more than the cross-plane effect. Therefore, heat transport becomes anisotropic, with the degree of anisotropy (ratio between in-plane and cross-plane thermal conductivity) increasing with strain. Furthermore, the degree of induced anisotropy is larger in compression than in tension at similar strains. Similar to the hydrostatic case, the relative changes in thermal conductivity are larger in compression.

The strain dependence in Fig. 4 can be qualitatively understood in part based on the lattice stiffness variation due to strain. A −3% compressive in-plane strain (plane strain conditions) leads to a 32% increase of the stiffness (15% for group velocity) in the in-plane directions, and to 29% in-

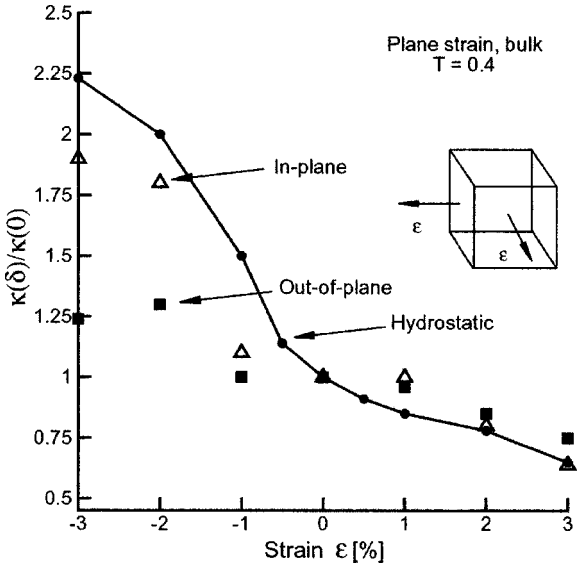

FIG. 4. Variation of the normalized in-plane (open symbols) and out-of-plane (filled symbols) thermal conductivity under plane strain conditions. The normalization is made with the bulk thermal conductivity corresponding to zero strain. The strain values on the horizontal axis represent strain in one in-plane direction (inset). The strain in the out-of-plane direction is zero. The values corresponding to hydrostatic loading (Fig. 3) are included for reference (line and cirlces). Under these loading conditions, the thermal conductivity becomes anisotropic.

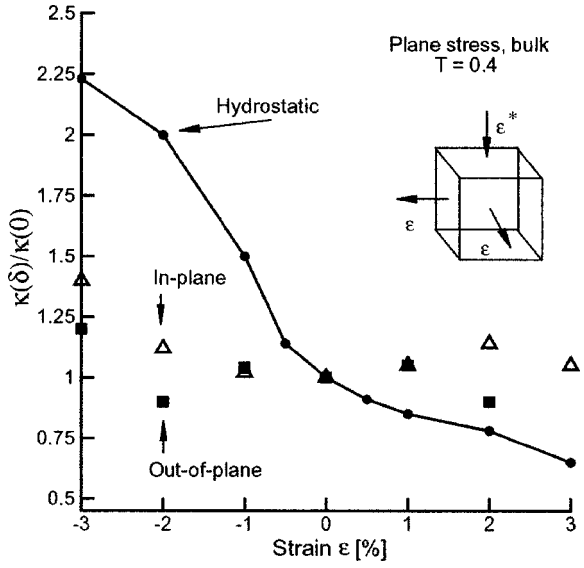

FIG. 5. Variation of the normalized in-plane (open symbols) and out-of-plane (filled symbols) thermal conductivity under plane stress conditions. The normalization is made with the bulk thermal conductivity corresponding to zero strain. The strain values on the horizontal axis represent strain in one in-plane direction (inset). The values corresponding to hydrostatic loading (Fig. 3) are included for reference (line and circles). The lattice thermal conductivity is essentially insensitive to the applied strain under these conditions.

crease in the out-of-plane direction (14% for group velocity). A tensile 3% strain in the in-plane directions corresponds to a reduction of 27% and 30% of the stiffness (15% and 16% for group velocity) in the in-plane and out-of-plane directions, respectively. As in the case of hydrostatic deformation, lattice anharmonicity appears to play a crucial role.

The plane stress case was considered next. The stress state in most nanostructures of current interest (thin films, superlattices, epitaxial islands on thin films, etc.) is essentially that of plane stress. In these cases, additional complexity is introduced by the presence of interfaces and free surfaces, the effects of strain and surface scattering overlapping. Here we study the two effects separately by first analyzing the influence of plane stress deformation on the lattice thermal conductivity in the bulk and then comparing with the size effect in unstrained films.

The plane stress deformation considered here is characterized by a biaxial in-plane strain state with strains ε in both directions, and an out-of-plane strain of magnitude $\varepsilon^* = -C_{1133}+C_{2233}/C_{3333}\varepsilon$. This relationship results from Hooke's law by imposing zero out-of-plane stress. Here, C_{ijkl} are components of the stiffness tensor. As before, the principal directions of strain are aligned with the cubic crystal axes and there is no coupling between normal and shear stress/strain components. In this coordinate system, the cubic symmetry requires $C_{1133}=C_{2233}$.

The variation of the lattice thermal conductivity with in-plane strain is rather marginal in this case, with the values departing only about 10%–20% from the conductivity of the bulk unloaded material (Fig. 5). Since this is also the magnitude of the error bar of present calculations, the only conclusion that can be drawn is that plane stress conditions influence thermal conductivity much less than other stress/strain states studied.

The stiffness variation with strain in both in-plane and out-of-plane directions is minor under this type of deformation. For example, -3% compressive in-plane strain leads to a 15% increase of the stiffness in the in-plane directions, and to a 9% increase in the out-of-plane direction, while a tensile 3% strain in the in-plane directions corresponds to a reduction of the stiffness in the in-plane and out-of-plane directions of only 2% and 8%, respectively. This observation establishes that, compared with the other strained configurations discussed above, the plane stress case corresponds to the least effect.

Finally, in order to assess the magnitude of the size effect in heat transport, a freestanding thin film was modeled. The model had ten lattice unit cells in the in-plane directions, with periodic boundary conditions being imposed. The sample has free surfaces in the out-of-plane direction (free standing film). The thermal conductivity was evaluated by similar means in both in-plane and out-of-plane directions in unstrained models of two, six and ten lattice unit cells thick. A major size effect was evidenced. The in-plane conductivity is three orders of magnitude smaller than that of the unstrained bulk. The out-of-plane value is one order of magnitude smaller than the in-plane one. As the model thickness is increased from two to ten unit cells, the thermal conductivity increases 2.5 times. The observed size effect is due to the intense scattering of phonons at film surfaces. Hence, in strained nanostructures under plane stress conditions, lattice thermal conductivity is controlled by boundary scattering. However, the change in mean free path induced by strain is expected to affect the magnitude of the size effect associated with dimensional scaling. Although for plane-stress condi-

tions the strain effect is minor, much larger mean free path changes could be induced under hydrostatic case. This may provide an effective way to control the thermal conductivity of nanostructures. The coupling between strain and size effects on heat transport in nanostructures requires further studies.

IV. CONCLUSIONS

The relative role of phonon boundary scattering and that of the strain state in controlling the lattice thermal conductivity in nanostructures was analyzed. Compressive strains induce an increase of thermal conductivity, while tensile strains lead to the opposite effect. The effect is most pronounced under hydrostatic loading and increases with strain. A nonhydrostatic strain state leads to thermal conductivity anisotropy. A smaller variation of the conductivity is observed in plane strain, while the effect in plane stress is negligible. These effects are due to strain induced changes of the group velocity (through material stiffness) and phonon mean free path (through lattice anharmonicity). The size effect was studied separately in unstrained films. Phonon scattering on surfaces leads to a dramatic reduction of the thermal conductivity effect which is much more important than that due to strain in the bulk. However, it is conjectured that strain may be used to tailor the phonon mean free path hence indirectly controlling the size effect. It is concluded that, although it is clear that dimensional scaling (phonon scattering) is the dominant factor leading to thermal conductivity reduction in nanostructures, the strain state may be used to control this property in some cases. This is especially true in nanostructures with dimensions below the critical thickness for dislocation nucleation that withstand residual strains much larger than the bulk.

[1] T. Fjeldly, T. Ishiguro, and C. Elbaum, Phys. Rev. B **7**, 1392 (1973).
[2] L. J. Challis and S. C. Haseler, J. Phys. C **11**, 4681 (1978).
[3] K. C. Sood and M. K. Roy, Phys. Rev. B **46**, 7486 (1992).
[4] A. Ramdane, B. Salce, and L. J. Challis, Phys. Rev. B **27**, 2554 (1983).
[5] Kh. I. Amirkhanov, Ya. B. Magomedov, S. N. Emirov, and R. M. Gadzhieva, Sov. Phys. Solid State **17**, 1956 (1976).
[6] Kh. I. Amirkhanov, Ya. B. Magedov, S. N. Emirov, and N. L. Kramynina, Sov. Phys. Solid State **21**, 1619 (1979).
[7] Kh. I. Amirkhanov, N. L. Kramynina, and S. N. Emirov, Sov. Phys. Solid State **25**, 1427 (1983).
[8] A. A. Averkin, Z. Z. Zhaparov, and L. S. Stilbans, Sov. Phys. Semicond. **5**, 1954 (1972).
[9] B. Hakansson and P. Andersson, J. Phys. Chem. Solids **47**, 355 (1986).
[10] J. Callaway, Phys. Rev. **113**, 1046 (1959).
[11] P. G. Klemens, Phys. Rev. **119**, 507 (1960).
[12] M. G. Holland, Phys. Rev. **132**, 2461 (1963).
[13] B. Abeles, Phys. Rev. **131**, 1906 (1963).
[14] K. Aflatooni and A. Nathan, Appl. Phys. Lett. **66**, 1110 (1995).
[15] M. Roufosse and P. G. Klemens, Phys. Rev. B **7**, 5379 (1973).
[16] S. Y. Ren and J. D. Dow, Phys. Rev. B **25**, 3750 (1982).
[17] G. Chen and M. Neagu, Appl. Phys. Lett. **71**, 2761 (1997).
[18] G. Chen, Phys. Rev. B **57**, 14958 (1998).
[19] P. Hyldgaard and G. D. Mahan, Phys. Rev. B **56**, 10754 (1997).
[20] S. Tamura, Y. Tanaka, and H. J. Maris, Phys. Rev. B **60**, 2627 (1999).
[21] M. V. Simkin and G. D. Mahan, Phys. Rev. Lett. **84**, 927 (2000).
[22] H. Berendsen, J. Postma, and J. W. van Gunsteren, J. Chem. Phys. **81**, 3684 (1984).
[23] J. M. Haile, *Molecular Dynamics Simulations* (Wiley, New York, 1985).
[24] P. K. Schelling, S. R. Phillpot, and P. Keblinski, Phys. Rev. B **65**, 144306 (2002).
[25] S. G. Voltz and G. Chen, Phys. Rev. B **61**, 2651 (2000).
[26] H. Kaburaki, J. Li, and S. Yip, Mater. Res. Soc. Symp. Proc. **538**, 503 (1991).
[27] Y. S. Touloukian, R. W. Powell, C. Y. Ho, and P. G. Klemens, *Thermophysical Properties of Matter* (Plenum, New York, 1970), Vol. 2.